THE JOURNAL OF PHYSICAL CHEMISTRY C

Article

pubs.acs.org/JPCC

Effects of Plasmonic Nanoparticle Incorporation on Electrodynamics and Photovoltaic Performance of Dye Sensitized Solar Cells

Julio Villanueva-Cab,* Jose Luis Montaño-Priede, and Umapada Pal

Instituto de Física, Benemérita Universidad Autónoma de Puebla, Apdo. Postal J-48, Puebla, Puebla 72570, Mexico

Supporting Information

ABSTRACT: Incorporation of plasmonic nanoparticles (NPs) has been considered recently to increase the absorption efficiency and/or the photocurrent of dye sensitized solar cells (DSSCs). However, metal NPs introduced in DSSCs make direct contact with iodide/triiodide-based liquid electrolyte, creating several problems such as recombination of charge-carriers, back reaction of photogenerated carriers, and corrosion of introduced metal NPs. For freshly prepared cells, charge-carrier recombination has been assumed as the principal process affecting the overall efficiency on DSSs. In this paper, through detailed optical and electrical characterization of gold nanoparticle-incorporated DSSCs and utilization of total electron density model, we demonstrate that the common perception that bare Au nanoparticles (NPs) act as recombination or back reactions centers cannot explain the photovoltaic behaviors of plasmonic DSSCs fully. Introduced plasmonic nanoparticles reduce electron injection efficiency in DSSCs, keeping the electron collection efficiency unchanged. Reduction of electron injection efficiency in plasmonic DSSCs is associated with an upward shift of the conduction band due to Au nanoparticle incorporation.

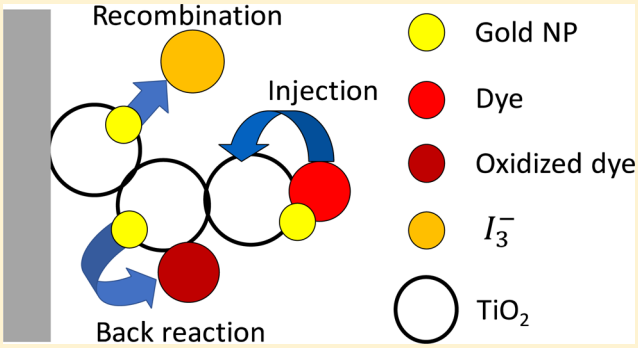

INTRODUCTION

Dye-sensitized solar cells (DSSCs) present an attractive alternative to traditional inorganic thin film devices due to their simpler manufacturing process and utilization of low purity components. Since the first report published on DSSC,[1] the field has expanded greatly; however, the efficiency of DSSC had stuck at a maximum of around 9% for most of its variants. This, in part, is due to distinct light absorption (by the dye molecules) and electron transport (in the nanostructured TiO_2) processes in DSSC, contrary to the single crystal solar cells, where both the light absorption and charge transport take place in the same material. On the other side, this also offers the advantage of incorporating new materials into a variety of photocollection systems to understand and maximize their effects. For example, different dyes,[2−4] quantum dots,[5,6] active layer materials of different morphologies (e.g., vertically aligned ZnO[7] or TiO_2 nanotubes[8,9]), and novel electrolyte solutions[10] have been tested to improve both the photocollection efficiency and electron transport of DSSCs. However, by employing new dyes or quantum dots as light absorber, and well-ordered structures as electrodes, the efficiency of DSSCs could only be improved marginally.[11] One of the most substantial improvement made in DSSCs in present time is through the incorporation of plasmonic nanostructures (typically silver or gold nanoparticles) through the enhancement of photo-absorption cross section of dye molecules. Plasmonic nanostructures of different geometries/morphologies have been tested for the enhancement of DSSC efficiency, exploiting the localized surface plasmon resonance (LSPR) characteristic of noble metal nanostructures.[12−19] Although the incorporation of "bare" Au nanoparticles as light-harvesting component in DSSCs has been shown to increase cells' photocurrent,[20] the use of corrosive iodide/triiodide-based liquid electrolyte and problems associated with recombination and back reaction of photogenerated carriers in DSSCs require the nanoparticles to be protected with a capping layer.[15,21−26]

Brown et al. have demonstrated a monotonic increase of light absorption with the amount of metal NPs incorporated into TiO_2 film, and at the same time, a monotonic decrease of the photocurrent, photovoltage, and fill factor in both solid state and electrolyte-based DSSCs.[21] The results led them to conclude that the direct contact between metal NPs, dye, and the electrolyte promotes recombination and back reaction of photogenerated carriers. As a consequence, different methods have been adopted to prevent the direct contact between metal NPs and the electrolyte in DSSCs.[15,21−26] However, to the best of our knowledge, the assumption that uncapped metal nanoparticles work as recombination centers in nanostructured electrodes of DSSCs has not been quantitatively studied in detail, and a clear understanding of the charge transfer kinetics in DSSCs on incorporating metal NP as light-harvesting component is lacking. In this work, we combine the use of a

Received: January 31, 2016
Revised: April 28, 2016
Published: April 29, 2016

DOI: 10.1021/acs.jpcc.6b01053
J. Phys. Chem. C 2016, 120, 10129−10136

well-established total electron density model and small perturbation measurements, providing a straightforward method to study the effect of plasmonic nanoparticle incorporation in DSSCs quantitatively.

EXPERIMENTAL METHODS

Materials. Trihydrated chloroauric acid ($HAuCl_4 \cdot 3H_2O$, ≥99.9%) and sodium citrate dihydrate ($Na_3C_6H_5O_7 \cdot 2H_2O$, 99%) were purchased from Sigma-Aldrich; sodium hydroxide pellets (NaOH, ACS grade) was purchased from JT Baker. Deionized water (>18.2 MΩ·cm) was obtained from a Millipore Simplicity system.

Synthesis and Characterization of Au Nanoparticles. Colloidal gold nanoparticles were synthesized by modified Turkevich's method. Briefly, 1 mL of 25 mM $HAuCl_4$ aqueous solution was added to 50 mL of deionized water in a round-bottom flask. The pH of the gold-ion solution was adjusted to 7.5 by dropwise addition of 1 M NaOH aqueous solution under magnetic stirring. Then, the solution was heated and refluxed at 100 °C, over a hot oil bath. On reaching this temperature, 3 mL of 17 mM sodium-citrate aqueous solution was added to the reaction mixture under vigorous stirring. The reaction continued for about 30 min at 100 °C, and then cooled down to room temperature naturally. On adding NaOH solution to the gold-ion solution, the characteristic yellow color of $AuCl_4^-$ solution gradually softened, finally turning colorless at pH 7.5, indicating the ligand substitution of Cl^- for OH^- in the gold complex. The color of the solution changed to violet after adding the citrate solution, and then to characteristic red, indicating the formation of gold nanoparticles. The pH of the reaction solution was measured by a Thermo Scientific, Orion Star pH meter. A Shimadzu, UV-3101PC double beam UV−vis-NIR spectrophotometer was used to record the absorption spectrum of the sample after it reached room temperature. The morphology and size of the nanoparticles were analyzed by a JEOL-JEM 211F transmission electron microscope, operating at 200 keV. The absorption spectrum of the colloidal sample (Figure S1 of Supporting Information) revealed characteristic surface plasmon resonance (SPR) absorption band of the nanoparticles peaked around 523 nm. The sample consists principally of quasi-spherical gold nanoparticles of 19.9 ± 2.7 nm average diameter (Supporting Information, Figure S2). High-resolution TEM micrographs of the sample revealed the formation of crystalline Au nanoparticles containing several structural defects (Supporting Information, inset of Figure S2a).

Fabrication of Au Nanoparticle-Incorporated DSSCs. A commercial paste (Dyesol 18NR-T) of TiO_2 nanocrystals was deposited onto transparent conducting oxide (TCO) coated glass substrates (F-doped SnO_2; 10 Ω/sq) through doctor-blade technique. After air-drying, the deposited layers were sintered in air at 500 °C for 1 h. The average thickness of the fabricated nanocrystalline TiO_2 layers was about 3.6 μm (measured by a Dektak II profilometer). Deposition of Au NPs over the annealed TiO_2 film surface was carried out by dispersing 20 μL of the colloidal solution of Au NPs and subsequent drying in air. The process was repeated for additional Au NP treatments as required. After annealing the TiO_2 + Au films again at 350 °C for 30 min and then cooling them to 80−100 °C, they were immersed in a solution of acetonitrile/*tert*-butyl alcohol (1:1, v/v) containing 0.3 mM Z907 dye for 15 h. The semitransparent counter electrodes were prepared by spreading two drops of 5 mM H_2PtCl_6 solution in 2-propanol over TCO substrates and their subsequent firing at 450 °C for 1 h. The TiO_2 + Au electrode and Pt-covered counter electrode were then sandwiched together using a 25 μm thick themoplastic (Surlyn, Dupont grade 1702). After introducing the electrolyte solution into the sandwiched electrodes, the predrilled holes of the counter electrode were sealed using small pieces of corning glass and thermoplastic. The electrolyte used in the DSSCs contained 0.6 M 1-butyl-3-methylimidazolium iodide and 0.03 M iodine in acetonitle/valeronitrile (85:15, v/v%).

Photovoltaic Characterization. Photovoltaic characterization of the fabricated cells was performed at room temperature using a setup consisting of a 450 W ozone-free Xe-lamp (Oriel) with a water filter, calibrated to an irradiance of 100 mW cm^{-2} at an equivalent air mass AM 1.5G on the surface of the solar cell; the intensity was calibrated using a certified 4 cm^2 monocrystalline silicon reference cell with incorporated KG-5 filter. No mask was used during the photovoltaic characterization of the DSSCs.

Small Perturbation Measurements. Steeped Light Induced Transient (SLIT) of photovoltage and photocurrent were measured to estimate the recombination lifetime and transport-time of the fabricated DSSCs, respectively.[27] The DSSCs were probed with a steeped modulated beam of 625 nm light (probe) superimposed on a relatively large background (bias) illumination also at 625 nm light. The probe and bias light entered the cells through the TCO substrate of the TCO +TiO_2 side. The photovoltage decay or transient photocurrent due to probe light was recorded and used to fit a single exponential decay with exponent $-t/\tau$ where τ is the fitting parameter termed electron lifetime or transport-time, respectively.[27,28] For the electron lifetime measurements, the photovoltage generated by the bias illumination (of a specific intensity) was considered as the average quasi-Fermi level of the DSSC electrode. Neutral density filters were used to vary the intensity of illumination, to generate a plot of electron lifetime as the function of photovoltage. Open circuit voltage and short circuit current were recorded for each illumination intensity. The steady state total electron density at specific illumination intensity was calculated under open circuit and short circuit conditions from the relation $n = \frac{J_{SC}\tau}{(1-P)\alpha q d}$[29] where J_{SC} is the short circuit photocurrent established by the bias light, τ is the electron lifetime or transport-time, P is the film porosity, α is the trap energy distribution parameter, q is the absolute value of the electron charge, and d is the TiO_2 film thickness.

THEORETICAL METHODS

The overall sunlight to electrical power conversion efficiency of DSSCs can be expressed by

$$\eta = \eta_{abs}\eta_{inj}\eta_{coll} \quad (1)$$

where η_{abs} is the efficiency of light absorption of the dye, η_{inj} is the efficiency of charge injection from the exited state of the dye to the conduction band of the TiO_2, and η_{coll} is the efficiency of charge collection in the mesoporous oxide layer (TiO_2), which is directly related to the transport and recombination properties of the TiO_2 film. Consequently, the main assumption that bare metal NPs act as recombination centers should have a detrimental effect on the η_{coll} and, hence, on the efficiency of solar cells. For instance, the short circuit photocurrent will also be directly affected across the η_{coll}. To

DOI: 10.1021/acs.jpcc.6b01053
J. Phys. Chem. C 2016, 120, 10129−10136

a)

Parameter	Value	Method
α'	0.114	From V_{oc} vs n
β	1.0	From V_{oc} vs τ_{rec}
b	3.308	From V_{oc} vs τ_{trans}
n_0 (m^{-3})	2.83 x10^{22}	From V_{oc} vs n
D_0 (m^2 s^{-1})	5.18 x10^{-11}	From V_{oc} vs τ_{trans}
k_0 (s^{-1})	0.818	From V_{OC}
η_{inj}	0.596	From J_{SC}
d (m)	3.6 x10^{-6}	Stylus Profilometry

b)

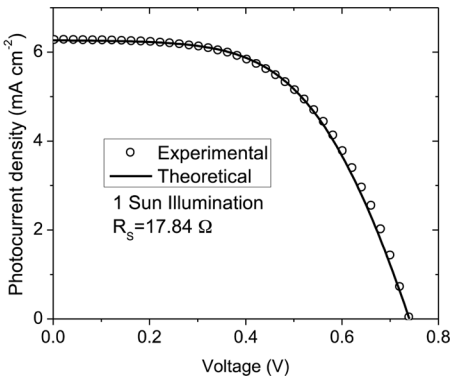

Figure 1. (a) Experimentally obtained input parameters for the reference DSSC, and (b) comparison between the measured current vs voltage curve and the theoretically obtained current vs voltage curve (obtained by solving the eq 1, using input parameters of the table) for the same DSSC.

evaluate the influence of Au NP incorporation in TiO_2 electrode on its charge collection properties, we combine the use of small perturbation measurements, current vs voltage curves, and a well-established numerical model. The physical model utilized in this work is based on the numerical integration of the continuity equation for electrons with appropriate generation, diffusion, and recombination terms as well as adequate boundary conditions. The model produces similar results to the widely used free electron density model.[30−32] Additionally, it makes possible to simultaneously simulate the steady state current vs voltage curves and time-dependent response of a DSSC using experimentally obtained parameters.[28] The continuity equation is solved in a linear geometry with x-coordinate being the distance to the TCO substrate (working electrode). The model assumes that transport occurs by multiple-trapping, so that the electron diffusion coefficient is a function of the total electron density. In addition, the kinetics of recombination to electron-acceptors such as tri-iodide ions or oxidized dye molecules is assumed to be electron density dependent. On the basis of this considerations, the continuity equation for electrons can expressed as[28]

$$\frac{\partial n}{\partial t} = \frac{\partial}{\partial x}\left[D_0(n/n_0)^{(1-\alpha)/\alpha}\frac{\partial n}{\partial x}\right] + G(x) - k_0(n/n_0)^{(\beta-\alpha)/\alpha}n \tag{2}$$

where n is time (t) and position (x) dependent; D_0 is the diffusion coefficient at a reference point (normally in the dark, which is denoted by the subscript zero); k_0 is the recombination rate in dark; α is the trap energy distribution coefficient; β is the nonlinear recombination factor, and $G(x)$ is the position-dependent generation term. The generation term can be calculated assuming a Lambert−Beer profile for light harvesting:

$$G(x) = \int_{\lambda_{min}}^{\lambda_{max}} \eta_{inj} I_0(\lambda)\alpha_{abs}[1 - \alpha_{abs}d]\exp\{\alpha_{abs}x\}\,d\lambda \tag{3}$$

where $I_0(\lambda)$ is the intensity of solar spectrum (standard AM1.5G) and α_{abs} is the absorption coefficient of the sensitized TiO_2 film in the DSSC at a specific wavelength λ. Note that by measuring the absorption spectrum of the sensitized TiO_2 film (η_{abs}) with and without plasmonic NPs, we are able to calculate a maximum expected photocurrent at short circuit for a DSSC assembled with those films under the assumption that $\eta_{coll} = \eta_{inj} = 1$. For simplicity, we assume that η_{inj} is independent of λ and n, even though there is experimental evidence that dye regeneration is a function of electron concentration, finally affecting η_{inj},[33,34] which will be used as a parameter to fit the experimental photocurrent at short circuit J_{SC} for known η_{coll}. It is important to mention that n in eq 2 is a generalized carrier density, and may therefore refer to a variety of situations as long as there is no drift contribution to carrier transport. For example, n is the excess electron density in a TiO_2 photoanode of a DSSC. The specific form of the diffusion and recombination terms and their corresponding parameters depend on the type of the cell, the nature of carrier transport, and the recombination processes. All the parameters in eq 2 can be estimated from small perturbation techniques such as Intensity Modulated Photocurrent Spectroscopy (IMPS), Intensity Modulated Photovoltage Spectroscopy (IMVS), Electrochemical Impedance Spectroscopy (EIS), transient/decay, and Stepped Light Induced Transient (SLIT) of photocurrent and photovoltage measurements, as has been demonstrated previously.[28,35−39] So, with adequate values of the input parameters, eq 2 can be solved numerically with appropriate boundary conditions, in order to obtain the total density profile as a function of time and position at a fixed voltage.[28,35−39] Consequently, we can calculate the (i) charge collection efficiency as a function of charge density (or illumination intensity); (ii) photocurrent density vs voltage curve, while performing a scan as a function of photovoltage; and (iii) photocurrent density vs time.

RESULTS AND DISCUSSION

To study the effect of plasmonic NP incorporation in the DSSC electrodes, we used a DSSC with no Au NP as reference. We have recently reported[35] a study of DSSCs with similar components (same TiO_2 paste, same dye but with different electrolyte) where all the input parameters used in the model, represented by eq 2, were obtained experimentally. To model the reference DSSC (Figure 1b), all the input parameters were obtained from SLIT of photovoltage and photocurrent measurements, current vs voltage curve, UV−vis spectroscopy and stylus profilometry. The electrodynamic parameters (Figure 1a) were obtained from SLIT of photovoltage and photocurrent measurements (see Supporting Information for details). The light harvesting was obtained from the absorption spectra of the sensitized TiO_2 films as shown in Figure 2b, and is used as input for the generation term in eq 3. We used the charge injection efficiency η_{inj} as a fitting parameter to fit the

DOI: 10.1021/acs.jpcc.6b01053
J. Phys. Chem. C 2016, 120, 10129−10136

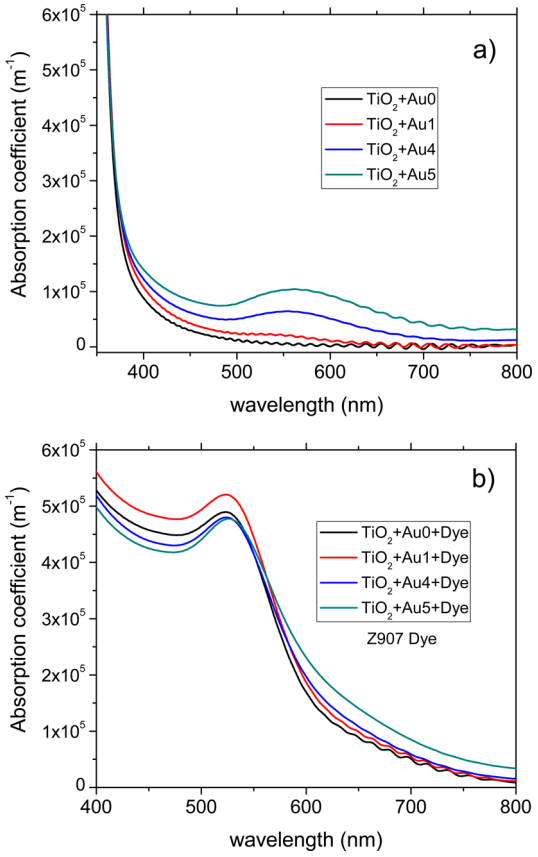

Figure 2. (a) Absorption spectra of four TiO_2 films (same thickness) with different Au treatments, and (b) absorption spectra of the same films sensitized with the Z907 dye.

experimental photocurrent under short circuit conditions at 1 Sun of illumination, with the assumption that the charge collection efficiency is 100%, i.e., under zero recombination. Then, the recombination rate in dark k_0 was used to fit the experimental voltage under open circuit conditions at 1 Sun of illumination. Note that when recombination is considered, we have to readjust the previously fitted values of η_{inj} and k_0 in order to reproduce the experimental short circuit photocurrent and open circuit voltage, respectively. Finally, a total series resistance R_S is used to fit the experimental maximum power generated by the DSSCs.

When we utilized all the fitting parameters of Figure 1a, eq 2 was solved for each voltage in the 0.0−0.740 V (the open circuit voltage of the reference DSSC) range to obtain the current−voltage curve for the reference DSSC (Figure 1b). For example, the theoretically calculated maximum efficiency value for the reference DSSC was about 6.4% with J_{SC} = 11.9 mA cm^{-2}, V_{OC} = 0.769 V, assuming a fill-factor (FF) of 0.7. For this calculation, we considered that (a) η_{inj} = 100%, (b) the absorption spectra for the TiO_2 + Au NPs + Dye film (reference) in Figure 2b, and (c) the input parameters of Figure 1a. Note that the highest reported efficiency for a DSSC with the same dye, a film thickness of 4.3 μm and a more complex electrolyte (compared with the one used in this study) was about 5.85%,[40] which is very close to the maximum efficiency calculated in this study. The consideration of η_{inj} = 100% is only used to establish a limit for the DSSC efficiency when electron recombination does not exist.

Figure 2 shows the effects of incorporating Au NPs in different concentrations on a TiO_2 film of about 3.6 μm thickness. As can be noticed in Figure 2a, the absorbance of the TiO_2 film increases gradually with increasing content of Au NPs. On the other hand, there appears a strong SPR peak around 560 nm in the absorption spectra. However, after sensitization, such a gradual increase of absorbance was not observed (Figure 2b). For the TiO_2 film with one Au NP treatment (red curve of Figure 2b), the overall intensity of the absorption band increased noticeably compared with the one with no Au NP treatment (black curve of Figure 2b), indicating an overall increase of light harvesting, increasing J_{SC} and V_{OC} in assembled devices. On the other hand, the intensity of the absorption band (around 560 nm) decreased marginally, extending its tail toward higher wavelengths for the films prepared with four and five Au NP treatments. While on incorporation of Au NPs at the surface of TiO_2 film reduces the surface area available for dye absorption, the increase of absorption intensity for the film after first Au NP treatment indicates that the presence of such a small amount of Au NPs at the surface does not affects its dye absorption capacity. For higher Au NP treatments, a higher number of Au NPs will be deposited at the film surface, reducing its effective surface area available for dye absorption. When the TiO_2 surface is largely covered by Au NPs, we can expect an increase in the recombination rate due to an increase of recombination centers. This is the case for the TiO_2 films with 4 and 5 Au NP treatments. However, the absorption spectra presented in Figure 2b could be used to calculate the effects of Au NP incorporation over the J_{SC} of DSSCs with the aid of eq 2 and the input data presented in Figure 1a.

The sensitized films with different Au NP treatments were used to fabricate DSSCs with the same electrolyte solution. As can be noticed in Figure 3a, there is not much improvement on the efficiency of the DSSCs by the incorporation of plasmonic NPs. A systematic decrease of J_{SC} and V_{OC} was observed for the samples with 0−4 Au NP treatments. This is a very common result and is frequently explained by the assumption that the metallic NPs act as recombination or back reaction centers.[21] On the other hand, the sample with 5 Au NP treatments revealed an increase in J_{SC} and V_{OC} with respect to the sample with 4 Au NP treatments. This increase might be due to the formation of a scattering layer at the top of the TiO_2 electrode due to the aggregation of Au NPs. Unfortunately, there is no straightforward method to determine whether the recombination process or the η_{inj}, which influences more the final efficiency of the Au NP incorporated DSSCs. To elucidate the earlier point, in the following section, we will evaluate how the incorporated Au NPs in TiO_2 nanostructures affect their: (1) light absorption or light harvesting efficiency, (2) recombination by decreasing the charge collection efficiency, and (3) the charge injection efficiency. The first point can be addressed as follow: if we assume that the only contribution of plasmonic NPs is the enhancement of absorption of TiO_2 films, as is observed in Figure 2b, we can expect some improvements in the J_{SC} and V_{OC} of DSSCs. Such improvements can be calculated by solving eq 2, utilizing the parameters of Figure 1a and the measured absorption spectra for the TiO_2 films with different Au NP treatments (Figure 2b). While the current−voltage behaviors of the DSSCs fabricated with and without Au NP incorporation are shown in Figure 3a, the theoretically estimated and experimentally obtained parameters (J_{SC} and V_{OC}) are compared in Figure 3b. As can be noticed from Figure

DOI: 10.1021/acs.jpcc.6b01053
J. Phys. Chem. C 2016, 120, 10129−10136

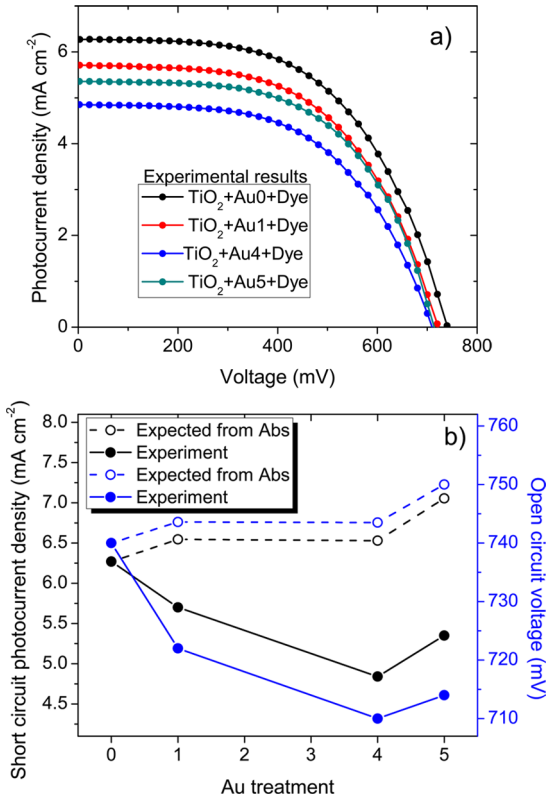

Figure 3. Effect of plasmonic NP incorporation on photovoltaic performance of DSSC: (a) experimental current vs voltage curves for different Au treatments to DSSC electrodes, (b) comparison between theoretical and experimentally obtained J_{SC} and V_{OC} values for the DSSCs fabricated with different Au NP treatments.

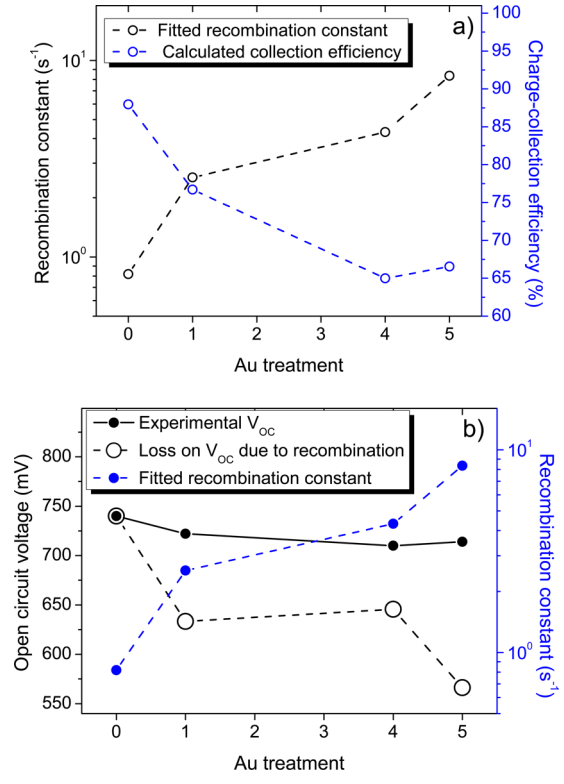

Figure 4. Effect of plasmonic NP incorporation on the recombination rate of DSSC: (a) the used k_0 to fit the experimental J_{SC}, (b) predicted effect of the fitted k_0 over V_{OC}.

3b, our assumption that the only contribution of Au NP incorporation is to improve the absorbance of TiO_2 films leads a gradual enhancement of J_{SC} and V_{OC}, contrary to experimental observations. This discrepancy between the theoretical and experimental results suggests an increase of the recombination rate or a decrease on charge collection efficiency of the plasmonic NP incorporated electrode, that finally affects the J_{SC} and V_{OC} of DSSC. To determine whether the incorporated Au NPs act as recombination centers in DSSC (2nd point), we repeated the calculations (used to obtain the results presented in Figure 3b) using the recombination constant k_0 as a fitting parameter to fit the experimental J_{SC} (solid black dots in Figure 3b), assuming that the incorporated Au NPs affect (enhance) the absorbance of TiO_2 film (Figure 2b), as well as act as recombination centers in assembled devices. It is important to note that here we are assuming that the transport properties of the TiO_2 electrodes is not largely affected by the incorporation of Au NPs, and there is no associated band shift.

Figure 4a shows the variations of recombination constant (black open circles) and charge-collection efficiency (blue open circles) of the cell with the incorporation of Au NPs, obtained using k_0 as fitting parameter to fit the experimental J_{SC}, i.e., assuming that incorporated Au NPs act as recombination centers, affecting the charge collection efficiency and finally decreasing the J_{SC} and V_{OC} of the DSSC. It is important to remember that this assumption is frequently made to justify the small improvement of DSSC efficiency observed on incorporation of metal NPs.[21] As can be noticed from Figure 4a, under this assumption, a gradual increase (1 order in magnitude) of the recombination rate constant (black open circles) with Au NP treatment is expected, leading to a maximum decrease of about 25% on the charge collection efficiency (blue open circles). As consequence, a maximum decrease of around 200 mV in V_{OC} is also expected (black open circles in Figure 4b) as it largely depends on the recombination rate constant. Contrary to this expectation, a maximum decrease of V_{OC} about 30 mV was measured (black dots in Figure 4b).

SLIT of photovoltage measurements were performed on the DSSCs with different Au NP treatments in order to determine the electron lifetime, a parameter that is directly related to the recombination rate constant. From these measurements, we can determine the variation of the recombination constant under the assumption that no band shift occurs. Figure 5a compares the lifetime measured for the DSSCs fabricated with different Au NP treatments. As we see, the consideration of no band edge shift results in about a maximum 3-fold increase in recombination rate (inverse of lifetime) between the cells prepared with no Au NP treatment and the cell prepared with 5 Au NP treatments at 0.45 V. However, a maximum 3-fold increase of the recombination rate within the measurements range does not agree with the estimated near 10-fold increase used to explain the decrease on J_{SC}. The results indicate that the observed decrease of J_{SC} and V_{OC} cannot be fully explained though the increase of recombination rate constant. Contribution of conduction band shift (and hence the variation of n_0), variation of electron trap distribution (and hence the parameter α), a change of transport properties (parameters D_0 and α), or even a change of recombination properties (k_0 and β parameters) might also be associated with the changes observed for J_{SC} and V_{OC}. As can be observed from Figure 5a, the slope

DOI: 10.1021/acs.jpcc.6b01053
J. Phys. Chem. C 2016, 120, 10129−10136

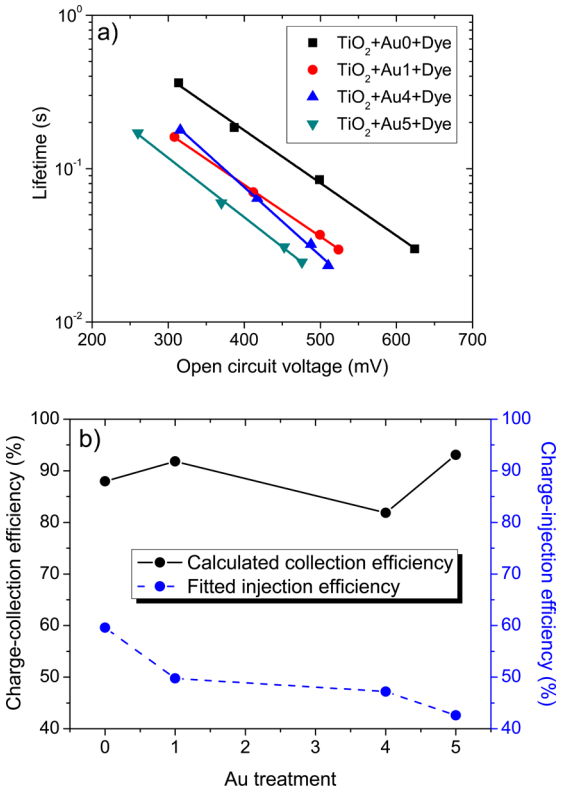

Figure 5. (a) Lifetime measurement as a function of the bias voltage for the Au treated DSSCs, (b) variations of the charge collection efficiency assuming the decrease in charge injection efficiency is due to Au NPs.

of the semilogarithmic plot of lifetime vs voltage is not the same for all the Au NP treatments, suggesting a variation in the nonlinear recombination parameter β, when the trap distribution α does not change. To evaluate whether Au NP incorporation affects other kinetic processes, we performed a complete characterization to obtain all the input parameters listed in Figure 1a for all the DSSCs. As can be seen in Table S1 of Supporting Information, there are no big variations (within the limit of fitting errors) for most of the input parameters as obtained by SLIT of photovoltage and photocurrent measurements (see Supporting Information for parameters extraction details). Contrary to the expectation, the variation of the slope of the semilogarithmic plot of lifetime vs voltage presented in Figure 5a is not due to a change of the nonlinear recombination parameter; instead, it is related to a decrease of the trap distribution parameter as shown in Table S1 (Supporting Information). However, such variations do not explain the decrease of J_{SC} and V_{OC} for DSSCs with Au NP incorporation.

The other parameter that also affects the J_{SC} of DSSCs is the charge injection efficiency. Recent publications[41] have shown that the efficiency of photoinduced electron transfer from sensitizers to semiconductors can be enhanced by coupling the sensitizer to plasmon resonance in metal nanoparticles. The extent of electron−plasmon coupling depends on the size and shape of metal NPs, and the dipole moments of the photosensitizer and metal NPs. As mentioned before, incorporated Au NPs can also alter the dye regeneration efficiency, finally affecting the charge injection efficiency.[28,33,34] Additionally, Au NP incorporation can also affect the contact between dye molecules and the TiO_2 surface, molecule conformation, aggregation, interaction between adjacent dye molecules, etc., affecting the charge injection efficiency. Under the assumption that the main effect of Au NP incorporation is to decrease the electron injection efficiency (3rd point), we used the electron injection efficiency as a fitting parameter to fit experimental J_{SC} as a function of Au NP treatments. In this calculation, we assumed that the incorporation of Au NPs affects: (a) the absorption efficiency or light harvesting capacity of TiO_2 film (as observed in Figure 2b) and (b) the charge injection efficiency in the DSSC, while utilizing parameters of Table S1 (Supporting Information). Figure 5b shows as the number of Au NP treatment increases, the value of the η_{inj} fitting the experimental J_{SC} and V_{OC} decreases. As we are using a different set of input parameters (experimentally obtained) for different Au NP treated DSSCs, it is not possible to compare their variations. However, the charge collection efficiency is a parameter that includes the contribution of all of them. From Figure 5b, we can see that the charge collection efficiency does not vary as systematically as the charge injection efficiency. In fact, on average the charge collection efficiency (from the fitting parameter obtained by SLIT of photovoltage and photocurrent) remains constant around 89% (with a standard deviation of 5%), while the charge injection efficiency gradually decreases from 60 to 43% with the increase of Au NP treatments. Accordingly, the variation of J_{SC} and V_{OC} observed experimentally (Figure 3b) can be fully explained considering a gradual decrease of η_{inj}, keeping the charge collection efficiency constant, and considering the variations of all the electrodynamic parameters involved in the model like: the recombination constant, the diffusion coefficient, the trap energy distribution coefficient, etc. For example, an upward shift of the conduction band, observed experimentally (Figure S4 in Supporting Information), could partly explain the decrease of the η_{inj} although it would lead to an increase of V_{OC}. However, the overall contribution of the electrodynamic parameters leads to a net decrease of V_{OC}. A further study on the effect of conduction band shift due to Au NP incorporation in TiO_2 electrode and its effect on η_{inj} is needed to understand the process.

CONCLUSIONS

Experimental and theoretical results obtained in this investigation indicate the common perception that bare Au NPs act as recombination or back reaction centers cannot explain the photovoltaic behaviors of plasmonic DSSCs fully. Instead, the observed variations of short circuit photocurrent and open circuit voltage can be fully explained by considering a decrease of electron injection efficiency associated with an upward shift of the conduction band, keeping the electron collection efficiency unchanged. However, other effects such as electron−plasmon coupling due to the formation metal NP aggregates over TiO_2 electrode at high gold nanoparticle concentrations may also affect the collection efficiency. This study highlights the importance of both mathematical tools and common DSSC characterization techniques to study the effects of plasmonic nanoparticle incorporation on DSSCs quantitatively. The mechanistic insight gained from this study on the electrodynamics and photovoltaic performance of DSSCs might be invaluable for the development of plasmonic dye sensitized solar cells of improved efficiency, and other plasmon based optoelectronic devices.

DOI: 10.1021/acs.jpcc.6b01053
J. Phys. Chem. C 2016, 120, 10129−10136

■ ASSOCIATED CONTENT

Supporting Information

The Supporting Information is available free of charge on the ACS Publications website at DOI: 10.1021/acs.jpcc.6b01053.

Absorption spectrum of the as-synthesized gold colloid; TEM micrograph of gold nanoparticles; SEM image of the TiO_2 + Au5 film; electron charge density vs open circuit voltage plots as a function of light intensity for samples with different Au NP treatments; electron transport-time vs open circuit voltage plots as a function of light intensity for samples with different Au NP treatments; electron transport-time vs charge density plots as a function of light intensity for samples with different Au NP treatments; electron lifetime vs open circuit voltage plots as a function of light intensity for samples with different Au NP treatments; list of fitting parameters obtained from SLIT of photovoltage and photocurrent measurements for the different Au treated DSSCs; comparison between the measured and theoretical current vs voltage curves for the DSSCs prepared with different Au NP treatments (PDF)

■ AUTHOR INFORMATION

Corresponding Author

*Tel: +52-222-229-5500, ext. 2064; e-mail: juliovc@ifuap.buap.mx.

Author Contributions

All authors contributed equally.

Notes

The authors declare no competing financial interest.

■ ACKNOWLEDGMENTS

The authors gratefully acknowledge CONACyT and VIEP-BUAP, Mexico, for financial supports. We acknowledge Gerko Oskam for access to photovoltaic characterization equipment.

■ REFERENCES

(1) O'Regan, B.; Gratzel, M. A Low-Cost, High-Efficiency Solar-Cell Based on Dye-Sensitized Colloidal TiO_2 Films. *Nature* **1991**, *353*, 737−740.

(2) Wang, P.; Zakeeruddin, S. M.; Moser, J. E.; Nazeeruddin, M. K.; Sekiguchi, T.; Grätzel, M. A Stable Quasi-Solid-State Dye-Sensitized Solar Cell with an Amphiphilic Ruthenium Sensitizer and Polymer Gel Electrolyte. *Nat. Mater.* **2003**, *2*, 402−407.

(3) Nazeeruddin, M. K.; Bessho, T.; Cevey, L.; Ito, S.; Klein, C.; De Angelis, F.; Fantacci, S.; Comte, P.; Liska, P.; Imai, H.; et al. A High Molar Extinction Coefficient Charge Transfer Sensitizer and its Application in Dye-Sensitized Solar Cell. *J. Photochem. Photobiol., A* **2007**, *185*, 331−337.

(4) Grätzel, M. Recent Advances in Sensitized Mesoscopic Solar Cells. *Acc. Chem. Res.* **2009**, *42*, 1788−1798.

(5) Mora-Seró, I.; Bisquert, J. Breakthroughs in the Development of Semiconductor-Sensitized Solar Cells. *J. Phys. Chem. Lett.* **2010**, *1*, 3046−3052.

(6) Sambur, J. B.; Novet, T.; Parkinson, B. A. Multiple Exciton Collection in a Sensitized Photovoltaic System. *Science* **2010**, *330*, 63−66.

(7) Law, M.; Greene, L. E.; Johnson, J. C.; Saykally, R.; Yang, P. Nanowire Dye-Sensitized Solar Cells. *Nat. Mater.* **2005**, *4*, 455−459.

(8) Zhu, K.; Neale, N. R.; Miedaner, A.; Frank, A. J. Enhanced Charge-Collection Efficiencies and Light Scattering in Dye-Sensitized Solar Cells Using Oriented TiO_2 Nanotubes Arrays. *Nano Lett.* **2007**, *7*, 69−74.

(9) Villanueva-Cab, J.; Jang, S.-R.; Halverson, A. F.; Zhu, K.; Frank, A. J. Trap-Free Transport in Ordered and Disordered TiO_2 Nanostructures. *Nano Lett.* **2014**, *14*, 2305−2309.

(10) Yella, A.; Lee, H.-W.; Tsao, H. N.; Yi, C.; Chandiran, A. K.; Nazeeruddin, M. K.; Diau, E. W-G.; Yeh, C.-Y.; Zakeeruddin, S. M.; Grätzel, M. Porphyrin-Sensitized Solar Cells with Cobalt (II/III)−Based Redox Electrolyte Exceed 12% Efficiency. *Science* **2011**, *334*, 629−634.

(11) Mathew, S.; Yella, A.; Gao, P.; Humphry-Baker, R.; Curchod, B. F. E.; Ashari-Astani, N.; Tavernelli, I.; Rothlisberger, U.; Nazeeruddin, M. K.; Grätzel, M. Dye-Sensitized Solar Cells with 13% Efficiency Achieved Through the Molecular Engineering of Porphyrin Sensitizers. *Nat. Chem.* **2014**, *6*, 242−247.

(12) Zhao, G. L.; Kozuka, H.; Yoko, T. Effects of the Incorporation of Silver and Gold Nanoparticles on the Photoanodic Properties of Rose Bengal Sensitized TiO_2 Film Electrodes Prepared by Sol-Gel Method. *Sol. Energy Mater. Sol. Cells* **1997**, *46*, 219.

(13) Wen, C.; Ishikawa, K.; Kishima, M.; Yamada, K. Effects of Silver Particles on the Photovoltaic Properties of Dye-Sensitized TiO_2 Thin Films. *Sol. Energy Mater. Sol. Cells* **2000**, *61*, 339.

(14) Hou, W.; Pavaskar, P.; Liu, Z.; Theiss, J.; Aykol, M.; Cronin, S. B. Plasmon Resonant Enhancement of Dye Sensitized Solar Cells. *Energy Environ. Sci.* **2011**, *4*, 4650.

(15) Qi, J. F.; Dang, X. N.; Hammond, P. T.; Belcher, A. M. Highly Efficient Plasmon-Enhanced Dye-Sensitized Solar Cells Through Metal@Oxide Core-Shell Nanostructure. *ACS Nano* **2011**, *5*, 7108.

(16) Zarick, H. F.; Hurd, O.; Webb, J. A.; Hungerford, C.; Erwin, W. R.; Bardhan, R. Enhanced Efficiency in Dye-Sensitized Solar Cells with Shape-Controlled Plasmonic Nanostructures. *ACS Photonics* **2014**, *1*, 806−811.

(17) Yen, Y.-C.; Chen, P.-H.; Chen, J.-Z.; Chen, J.-A.; Lin, K.-J. Plasmon-Induced Efficiency Enhancement on Dye-Sensitized Solar Cell by a 3D TNW-AuNP Layer. *ACS Appl. Mater. Interfaces* **2015**, *7*, 1892−1898.

(18) Xu, Q.; Liu, F.; Liu, Y.; Cui, K.; Feng, X.; Zhang, W.; Huang, Y. Broadband Light Absorption Anhancement in Dye-Sensitized Solar Cells with Au-Ag Alloy Popcorn Nanoparticles. *Sci. Rep.* **2013**, *3*, 2112.

(19) Chang, S.; Li, Q.; Xiao, X.; Wonga, K. Y.; Chen, T. Enhancement of Low Energy Sunlight Harvesting in Dye-Sensitized Solar Cells Using Plasmonic Gold Nanorods. *Energy Environ. Sci.* **2012**, *5*, 9444−9448.

(20) Ishikawa, K.; Wen, C. J.; Yamada, K.; Okubo, T. The Photocurrent of Dye-Sensitized Solar Cells Enhanced by the Surface Plasmon Resonance. *J. Chem. Eng. Jpn.* **2004**, *37*, 645.

(21) Brown, M. D.; Suteewong, T.; Kumar, R. S. S.; D'Innocenzo, V.; Petrozza, A.; Lee, M. M.; Wiesner, U.; Snaith, H. J. Plasmonic Dye-Sensitized Solar Cells Using Core-Shell Metal-Insulator Nanoparticles. *Nano Lett.* **2011**, *11*, 438−445.

(22) Gangishetty, M. K.; Lee, K. E.; Scott, R. W. J.; Kelly, T. L. Plasmonic Enhancement of Dye Sensitized Solar Cells in the Red-to-near-Infrared Region using Triangular Core−Shell Ag@SiO_2 Nanoparticles. *ACS Appl. Mater. Interfaces* **2013**, *5*, 11044−11051.

(23) Sheehan, S. W.; Noh, H.; Brudvig, G. W.; Cao, H.; Schmuttenmaer, C. A. Plasmonic Enhancement of Dye-Sensitized Solar Cells Using Core−Shell−Shell Nanostructures. *J. Phys. Chem. C* **2013**, *117*, 927−934.

(24) Jang, Y. H.; Jang, Y. J.; Kochuveedu, S. T.; Byun, M.; Lin, Z.; Kim, D. H. Plasmonic Dye-Sensitized Solar Cells Incorporated with Au−TiO_2 Nanostructures with Tailored Configurations. *Nanoscale* **2014**, *6*, 1823−1832.

(25) Dang, X.; Qi, J.; Klug, M. T.; Chen, P.-Y.; Yun, D. S.; Fang, N. X.; Hammond, P. T.; Belcher, A. M. Tunable Localized Surface Plasmon-Enabled Broadband Light-Harvesting Enhancement for High-Efficiency Panchromatic Dye-Sensitized Solar Cells. *Nano Lett.* **2013**, *13*, 637−642.

(26) Erwin, W. R.; Zarick, H. F.; Talbert, E. H.; Bardhan, R. Light Trapping in Mesoporous Solar Cells with Plasmonic Nanostructures. *Energy Environ. Sci.* **2016**, DOI: 10.1039/C5EE03847B.

DOI: 10.1021/acs.jpcc.6b01053
J. Phys. Chem. C 2016, 120, 10129−10136

(27) Nakade, S.; Kanzaki, T.; Wada, Y.; Yanagida, S. Stepped Light-Induced Transient Measurements of Photocurrent and Voltage in Dye-Sensitized Solar Cells: Application for Highly Viscous Electrolyte Systems. *Langmuir* **2005**, *21*, 10803−10807.
(28) Anta, J. A.; et al. A Continuity Equation for the Simulation of the Current−Voltage Curve and the Time-Dependent Properties of Dye-Sensitized Solar Cells. *Phys. Chem. Chem. Phys.* **2012**, *14*, 10285−10299.
(29) van de Lagemaat, J.; Frank, A. J. Nonthermalized Electron Transport in Dye-Sensitized Nanocrystalline TiO_2 Films: Transient Photocurrent and Random-Walk Modeling Studies. *J. Phys. Chem. B* **2001**, *105*, 11194−11205.
(30) Peter, L. M. Characterization and Modeling of Dye-Sensitized Solar Cells. *J. Phys. Chem. C* **2007**, *111*, 6601−6612.
(31) Södergren, S.; Hagfeldt, A.; Olsson, J.; Lindquist, S. E. Theoretical Models for the Action Spectrum and the Current-Voltage Characteristics of Microporous Semiconductor Films in Photoelectrochemical Cells. *J. Phys. Chem.* **1994**, *98*, 5552−5556.
(32) Bisquert, J.; Vikhrenko, V. S. Interpretation of the Time Constants Measured by Kinetic Techniques in Nanostructured Semiconductor Electrodes and Dye-Sensitized Solar Cells. *J. Phys. Chem. B* **2004**, *108*, 2313−2322.
(33) Jennings, J. R.; Liu, Y.; Wang, Q. Efficiency Limitations in Dye-Sensitized Solar Cells Caused by Inefficient Sensitizer Regeneration. *J. Phys. Chem. C* **2011**, *115*, 15109−15120.
(34) Li, F.; Jennings, J. R.; Wang, Q. Determination of Sensitizer Regeneration Efficiency in Dye-Sensitized Solar Cells. *ACS Nano* **2013**, *7*, 8233−8242.
(35) Villanueva-Cab, J.; Anta, J. A.; Oskam, G. The Effect of Recombination under Short-Circuit Conditions on the Determination of Charge Transport Properties in Nanostructured Photoelectrodes. *Phys. Chem. Chem. Phys.* **2016**, *18*, 2303−2308.
(36) Guillen, E.; Ramos, F. J.; Anta, J. A.; Ahmad, S. Elucidating Transport-Recombination Mechanisms in Perovskite Solar Cells by Small-Perturbation Techniques. *J. Phys. Chem. C* **2014**, *118*, 22913−22922.
(37) Anta, J. A.; Casanueva, F.; Oskam, G. A Numerical Model for Charge Transport and Recombination in Dye-Sensitized Solar Cells. *J. Phys. Chem. B* **2006**, *110*, 5372−5378.
(38) Villanueva-Cab, J.; Oskam, G.; Anta, J. A. A Simple Numerical Model for the Charge Transport and Recombination Properties of Dye-Sensitized Solar Cells: A Comparison of Transport-Limited and Transfer-Limited Recombination. *Sol. Energy Mater. Sol. Cells* **2010**, *94*, 45−50.
(39) Villanueva, J.; Anta, J. A.; Guillen, E.; Oskam, G. Numerical Simulation of the Current-Voltage Curve in Dye-Sensitized Solar Cells. *J. Phys. Chem. C* **2009**, *113*, 19722−19731.
(40) Cao, Y.; Bai, Y.; Yu, Q.; Cheng, Y.; Liu, S.; Shi, D.; Gao, F.; Wang, P. Dye-Sensitized Solar Cells with a High Absorptivity Ruthenium Sensitizer Featuring a 2-(Hexylthio)thiophene Conjugated Bipyridine. *J. Phys. Chem. C* **2009**, *113*, 6290−6297.
(41) Ramakrishna, S.; Pelton, M.; Gray, S. K.; Seideman, T. Plasmon-Enhanced Electron Injection in Dye-Sensitized Solar Cells. *J. Phys. Chem. C* **2015**, *119*, 22640−22645.

DOI: 10.1021/acs.jpcc.6b01053
J. Phys. Chem. C 2016, 120, 10129−10136